Astronomy & Astrophysics manuscript no. Dormant˙binaries˙v2
October 8, 2010

A search for dormant binaries with degenerate components in ω Centauri and NGC 6397

M. Rozyczka[1], J. Kaluzny[1], P. Pietrukowicz[1,2], W. Pych[1], M. Catelan[2], C. Contreras[2], and I. B. Thompson[3]

[1] Nicolaus Copernicus Astronomical Center, ul. Bartycka 18, 00-716 Warszawa, Poland
[2] Pontificia Universidad Católica de Chile, Departamento de Astronomía y Astrofísica, Av. Vicuña MacKenna 4860, 782-0436 Macul, Santiago, Chile
[3] Carnegie Institution of Washington, 813 Santa Barbara Street, Pasadena, CA 91101, USA

Received ...; accepted ...

ABSTRACT

Aims. We report on the first spectroscopic search for quiescent degenerate binaries in globular clusters.
Methods. Our survey is based on a sample of short-period optical variables which are likely optical counterparts of quiescent X-ray sources in ω Centauri (NGC 5139) and NGC 6397.
Results. The studied candidates have nearly sinusoidal light curves with amplitudes of 0.05–0.12 mag in V (0.35 mag in one case), and periods of 0.1–1.3 days. This type of variability, most probably originating from the ellipsoidal effect, has been observed in X-ray novae when they settled into quiescence after an outburst.
Conclusions. We find that two of the surveyed systems harbour dim components with masses in excess of 1 $M_{\odot}$, making them attractive targets for future investigations. We also suggest that there are two subpopulations of blue stragglers in ω Centauri, differing in mass-transfer history and/or helium content.

Key words. globular clusters: individual: NGC 5139 (ω Centauri), NGC 6397 – binaries: close – binaries: spectroscopic – blue stragglers

1. Introduction

Since the early surveys with the Uhuru and OSO-7 satellites it has been known that X-ray sources occur about a thousand times more frequently in globular clusters (GCs) than in the rest of the Galaxy (e.g., Katz 1975; Clark 1975). Over fifteen hundred of them have been detected to date in these stellar systems by recent missions such as Chandra and XMM-Newton (Pooley 2010, and references therein). In addition, over a hundred millisecond pulsars – objects which have evolved in low-mass X-ray binaries – are known to reside in GCs (Lynch et al. 2010). Most of the X-ray sources are binaries with degenerate components (neutron stars or white dwarfs), henceforth referred to as "degenerate binaries". Remarkably, no stellar-mass black holes (BH) are known in Galactic GCs, despite theoretical predictions that they should exist (e.g., Devecchi et al. 2007). The presence of intermediate-mass black holes (IMBHs) ($100\,M_{\odot} < M < 10^{3-4}\,M_{\odot}$) in GCs has also not yet been proven (e.g., Maccarone & Servillat 2008; van der Marel & Anderson 2010).

While the origin of IMBHs is unclear, stellar-mass black holes should form along with neutron stars via supernova explosions during the early evolution of a cluster. The very presence of such objects would **provide** interesting information concerning the effectiveness of dynamical interactions leading to the ejection of BHs into the intracluster medium, which according to the predictions of current approximate models should be very high (e.g., Downing et al. 2010). Their absence would confirm those predictions. Alternatively, it could mean that massive low-metallicity stars cannot produce BHs, which would have important implications for the origin of early BHs, believed to be seeds for the first galaxies in the Universe. In either case, searching for black holes in GCs is certainly a worthwhile task.

It is well known that field X-ray novae (binaries most probably hosting stellar-mass black holes) spend most of their time in quiescence, showing only ellipsoidal variability in the visible domain (Remillard & McClintock 2006). Since GCs harbor a multitude of degenerate binaries, they must also contain many systems which presently accrete at a very low rate or do not accrete at all, thus being very weak or undetectable in the X-rays. Based on X-ray luminosity (L_X) and hardness ratio, Grindlay (2006) splits the population of weak X-ray sources in GCs into four major classes. The first three, arranged according to L_X increasing from 10^{29} (the present sensitivity limit for the nearest GCs) to 10^{32} erg s^{-1} are i) active binaries (binary main-sequence stars in which the X-ray emission originates from chromospheric activity, e.g. BY Dra type systems); ii) cataclysmic variables (in which a white dwarf accretes from a low-mass main-sequence companion); iii) quiescent low-mass X-ray binaries (in which a neutron star intermittently accretes from a main-sequence or evolved companion), hereafter referred to as qLMXBs. The fourth class is composed of millisecond pulsars, whose luminosity strongly depends on the predominant mechanism generating X-ray quanta (residual accretion; collision of the pulsar wind with the ambient medium or with matter lost by the companion; thermal surface emission).

The study of weak X-ray sources is hampered by the fact that even in the nearest GCs they are detected down to the present sensitivity limit, and often remain unclassified as they are too dim to allow for an estimate of the hardness ratio. Most of them are likely active binaries or cataclysmic variables, but some may be quiescent systems with neutron stars or even black holes.

Send offprint requests to: M. Rozyczka,
e-mail: mnr@camk.edu.pl

Optical counterparts of these systems are often weak and hard to identify in the crowded GC environment (e.g., Verbunt et al. 2008). So far, the X-ray data have allowed us to identify a few candidate qLMXBs, but their nature has not been confirmed by optical spectroscopy (Guillot et al. 2009).

We decided to follow an entirely different approach. Instead of looking for optical counterparts of X-ray sources, we select a sample of candidate systems for degenerate binaries from short-period, low-amplitude optical variables catalogued in existing surveys, and measure their radial velocities. Our targets have nearly sinusoidal light curves with V-band amplitudes smaller than 0.35 mag and periods shorter than ∼1.3 days. This type of variability is common in all classes of close degenerate binaries; in particular, it is observed in optical counterparts of several Galactic X-ray novae which almost certainly harbor BHs (Remillard & McClintock 2006). The optical modulation is induced mostly by the ellipsoidal effect from the nondegenerate component, with an amplitude depending mainly on the Roche lobe filling factor and the inclination of the orbit. Close degenerate binaries can be unambiguously identified as single-line systems with large orbital velocities ($K > 150$ km s^{-1}). Among them, those harboring a black hole are distinguished by a mass function $f_m = (m \sin i)^3/(m_{bin})^2 > 2M_\odot$, where m_{bin} and m stand for the total mass of the binary and the mass of one of its components (Remillard & McClintock 2006).

Our sample and observational data are introduced in Sect. 2. A detailed analysis of the data is reported in Sect. 3, and the results are discussed in Sect. 4.

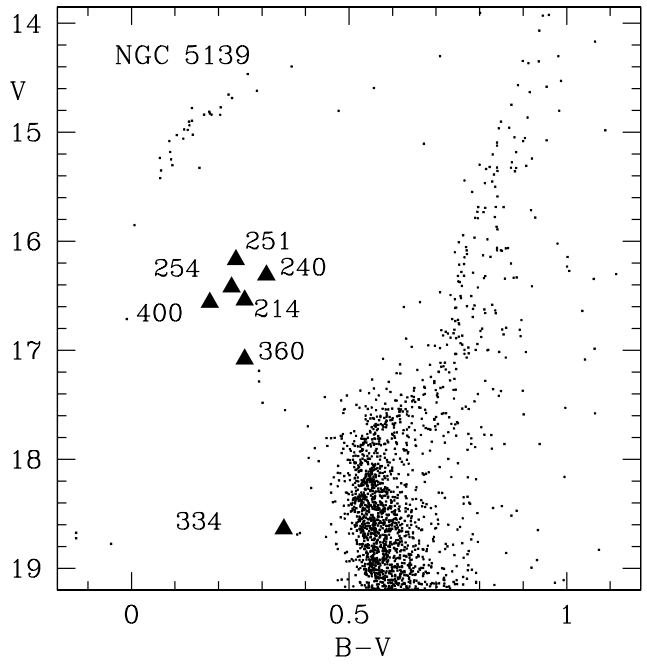

Fig. 1. Color-magnitude diagram of ω Cen based on CASE data (Kaluzny et al. 2004) transformed to the BV system with the help of standards listed by Stetson (2000). Marked are the locations of the investigated systems.

2. Observations and data reduction

Optical counterparts of active X-ray sources in GCs have been found essentially everywhere in color-magnitude diagrams: to the left of the main sequence, on the main sequence, to the right of it, on subgiant, giant and horizontal branches, and also above the main-sequence turnoff in the regions occupied by blue stragglers and EHB stars (e.g. Heinke et al. 2005; Servillat et al. 2008). Thus, while preparing this study we felt it justified to pick photometrically suitable targets without paying attention to their location with respect to the main sequence. Since large-amplitude variables are more likely to be ordinary contact binaries, we avoided objects with full V-band amplitudes in excess of ∼0.35 mag. Suspected pulsating variables were excluded; we also took care to exclude systems with appreciable X-ray emission. Where it was possible, the membership status of the target was established based on the data of Bellini et al. (2009) for ω Cen, and Anderson (priv. comm.) and Strickler et al. (2009) for NGC 6397. In the remaining cases membership was decided *a posteriori* based on the systemic velocity with respect to the cluster.

Alltogether, we selected seven objects in ω Cen and four in NGC 6397. In color-magnitude diagrams two of them are located to the left of the main sequence, seven above the main-sequence turnoff, and two at the turnoff itself (see Figs. 1 and 2). A summary of their basic data is given in Table 1 (the labels are the same as those introduced by Kaluzny et al. (2004) for ω Cen and Kaluzny et al. (2006) for NGC 6397).

Our paper is based on photometric measurements of Kaluzny et al. (2004, 2006), supplemented by those of Weldrake et al. (2007) and by our unpublished data for NGC 6397 obtained on the du Pont telescope at Las Campanas Observatory, Chile (a total of 771 V-band frames was acquired between 2009 June 20 and June 30, and reduced in the same way as in Kaluzny et al. (2006)). The newer data demonstrated that the observed light variations were coherent, although in some cases the light curve was changing from symmetric to asymmetric or vice versa.

Spectroscopic data were collected during the nights 20/21 and 21/22 of May 2009 with the MagE (Magellan Echellette) spectrograph attached to the 6.5-m Magellan-Clay telescope at Las Campanas Observatory. The seeing varied betweeen 0.″5 and 0.″8 on the first night, and betweeen 0.″4 and 0.″9 on the second one. A 0.″85 slit was used, providing a resolution $R = 4820$.

During the observations pairs of scientific spectra taken for the same target were separated by an exposure of a thorium-argon hollow-cathode lamp. The exposure times per spectrum ranged from 120 s to 1080 s, depending on object brightness and observing conditions. After bias and flat-field correction each pair of frames was combined into a single frame, allowing for the rejection of cosmic ray hits. The observations were reduced with the IRAF[1] ECHELLE package.

In order to determine the mass function of a given target it was sufficient to take just a few spectra at different phases, and fit a simple sinusoid to its velocity curve phased with the photometric ephemeris. Altogether, 96 spectra were obtained (from 5 to 10 per object). The useful range of the reduced spectra extended from 4050 Å to 6800 Å, where the spectra had $13 < S/N < 23$ (with a few cases of lower quality). Radial velocities were measured in that range with the help of IRAF routines FXCOR and XCSAO, using synthetic templates from the library compiled by Munari et al. (2005). The results were verified by applying the broadening function formalism described by Rucinski (2002). In most cases the differences between various measurements were

[1] IRAF is distributed by the National Optical Astronomy Observatories, which are operated by the AURA, Inc., under cooperative agreement with the NSF.

Table 1. Basic information on the target objects.

Cluster	Star	α_{2000} [h:m:s]	δ_{2000} [°:′:″]	p_m*	L_X** [10^{30} erg s^{-1}]	V [mag]	$B-V$ [mag]	ref.†
ω Cen	V214	13:27:21.82	−47:37:19.0	97	<13	16.55	0.25	1,2
ω Cen	V240	13:27:28.68	−47:26:19.5	99	<1.2	16.31	0.30	1,2
ω Cen	V251	13:27:28.02	−47:26:43.7	97	<1.2	16.17	0.25	1
ω Cen	V254	13:27:28.61	−47:27:39.0	99	<1.2	16.41	0.25	1,2
ω Cen	NV334	13:27:23.39	−47:29:11.9	88	<1.2	18.63	0.35	1
ω Cen	NV360	13:26:02.06	−47:32:23.6	100	<1.2	17.09	0.25	1
ω Cen	NV400	13:26:10.09	−47:31:50.3	99	<1.2	16.56	0.20	1
NGC 6397	V17	17:40:43.78	−53:41:16.2	100	0.4	16.17	0.40	3,4
NGC 6397	V20	17:40:41.66	−53:40:33.1	100	1.6	15.75	0.40	3,4
NGC 6397	V27	17:41:13.80	−53:41:14.1	-	-	18.19	0.45	3,4
NGC 6397	V36	17:40:44.10	−53:42:11.3	-	0.4	16.48	0.60	3,4

* Membership probability: Bellini et al. (2009) for V214-NV400; Strickler et al. (2009) and Anderson (2010, priv. comm.) for V17-V20; no data available for V27 and V36.
** X-ray luminosity: Gendre et al. (2003) for V214; Haggard et al. (2004) for V240-NV400; Bogdanov et al. (2010) for V17-V20 and V36; no data available for V27.
† Photometry: 1 - Kaluzny et al. (2004); 2 - Weldrake et al. (2007); 3 - Kaluzny et al. (2006); 4 - our unpublished data collected in 2009.

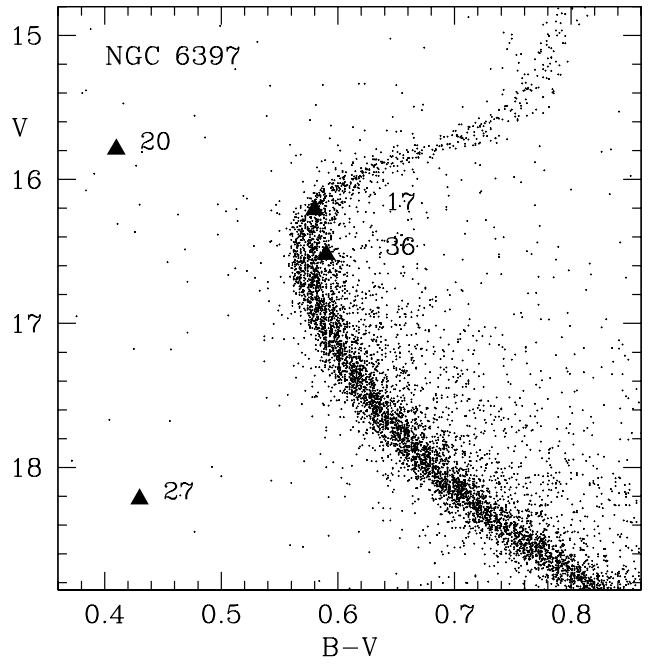

Fig. 2. Color-magnitude diagram of NGC 6397 (after Kaluzny et al. 2006) with marked positions of the investigated systems.

smaller than $\Delta v = 10$ km s^{-1}, which may be regarded as a fair estimate of the error.

3. Analysis

While our data are insufficient for a detailed analysis, an estimate of the basic parameters of the observed systems is possible. In all cases but one (V20 in NGC6307) single-line spectra are observed, indicating that to a first approximation all the light we receive from the binary is produced by just one of the components. Based on this assumption, we may set some limits for acceptable configurations.

3.1. Method

Our observables are: orbital period P, apparent V-band magnitude V, color index $B-V$, amplitude of the light curve ΔV_{obs}, and amplitude of the velocity curve K_{obs}. Since the distance moduli to ω Cen and NGC 6397 are known, V of a system belonging to the cluster is equivalent to the observed bolometric magnitude of its visible component M^o_{bol} ("observed" means here "derived from observations; hence index "o"). We adopt $(m-M)_0 = 13.75$ mag and $E(B-V) = 0.115$ mag for ω Cen (Villanova et al. 2007, and references therein), and $(m-M)_0 = 12.03$ mag and $E(B-V) = 0.183$ mag for NGC 6397 (Richer et al. 2008, and references therein). Assuming $A_V = 3.1\,E(B-V)$, the corresponding values of A_V are 0.36 mag and 0.57 mag, yielding a distance modulus $(m-M)_V$ of 14.11 mag for ω Cen and 12.60 mag for NGC 6397.

The effective temperature of the visible component T is known from the relation between the color index $B-V$ and temperature derived for an appropriate chemical composition. We adopt [Fe/H] = −1.8 for ω Cen (Sollima et al. 2009) and [Fe/H] = −2.0 for NGC 6397 (Carretta et al. 2009), and we use color transformation tables provided by Lejeune et al. (1998). The parameters derived for our target stars from the observational data are given in Table 2.

The last column in Table 2 contains mass-center velocities with respect to the cluster obtained by a simple sinusoid fit, with heliocentric velocities of the clusters (232.3 km s^{-1} for ω Cen and 18.9 km s^{-1} for NGC 6397) taken from the catalogue compiled by Harris (1996) and updated online.[2] The velocities of V214, V240, and V254 may seem a bit largish for their distances from the cluster center (17′.0, 14′.9, and 14′.7, respectively), even though the published cluster tidal radius is $r_t = 44'.8$ (Trager et al. 1995), or $r_t = 57'.03$ according to the Harris (1996) catalog. That these stars are well within the limits for cluster membership is confirmed by Fig. 6 in Sollima et al. (2009), which shows the variation in radial velocity of ω Cen stars as a function of distance from the cluster center. Still, V240 turned out to be a doubtful case (see Sect. 3.3.1). As for V214 and V254, we checked that the best fits described in Sect. 3.3.1 were not affected when v_0 was lowered, respectively, to 10 and

[2] http://www.physics.mcmaster.ca/Globular.html

Table 2. Parameters of the target objects derived from the observations.

Cluster	Star	P [d]	M^o_{bol} [mag]	T [K]	K_{obs} [km s^{-1}]	f_m [$M_\odot$]	v_0 [km s^{-1}]
ω Cen	V214	0.341806	2.44	8300	35	1.5×10^{-3}	21
ω Cen	V240	0.331888	2.19	8000	< 10	$< 3.4\times10^{-5}$	21
ω Cen	V251	0.922458	2.06	8300	35	4.1×10^{-3}	6
ω Cen	V254	0.385071	2.30	8300	60	8.0×10^{-3}	18
ω Cen	NV334	0.257881	4.52	7300	35	1.1×10^{-3}	−9
ω Cen	NV360	0.630821	2.98	8300	45	5.9×10^{-3}	−17
ω Cen	NV400	0.636874	2.40	8800	20	5.3×10^{-4}	−7
NGC 6397	V17	1.061316	3.35	6200	50	1.4×10^{-2}	−2
NGC 6397	V20	0.861177	2.94	7200	*	*	9
NGC 6397	V27	0.556134	5.38	7500	25	9.0×10^{-4}	−6
NGC 6397	V36	1.098569	3.65	6200	95	9.7×10^{-2}	−1

* Velocities of both components were measured, yielding $K_1 = 25$ km s^{-1} and $K_2 = 130$ km s^{-1}. The corresponding mass functions are $f_{m1} = 1.4\times10^{-3}\ M_\odot$ and $f_{m2} = 1.9\times10^{-1}\ M_\odot$.

6 km s^{-1}. The velocity of NV360, although also rather large, is entirely consistent with the distance of this system from the center of ω Cen (3.′6), at which the relative velocities of cluster members reach ±35 km s^{-1} (Sollima et al. 2009).

With T being fixed, the task is to find the orbital separation a, inclination of the orbit i, and masses of the components m_1 and m_2. Unless indicated otherwise, we assume that the system is semi-detached, with the visible component filling its Roche lobe. It must be stressed here that this particular model of the binary *is not related to the physical structure of our targets* (in fact, in some cases it might imply a mass transfer unstable on a dynamical scale). A semi-detached system is simply the most compact one among those with $M^c_{bol} = M^o_{bol}$. Focusing on it, we minimize the orbital separation, so that the corresponding "semi-detached" masses m^{sd}_1 and m^{sd}_2 are the smallest allowable given P and q. The lower limits of the actual masses of the components are obtained by finding "the best" mass ratio q_b, defined as the one for which $\Delta V_c/\Delta V_{obs} = 1$ (see Sect. 3.2 for further discussion). Our analysis involves the following steps:

1. Specify if the visible component is primary or secondary.
2. Set the mass ratio $q \equiv m_2/m_1 < 1$ (we define the primary as the more massive component, not necessarily being the more luminous one).
3. Given the orbital period P, adjust the separation a so that the calculated bolometric magnitude M^c_{bol} of the visible component be equal to M^o_{bol}.
4. Adjust i and v_0 so that the calculated velocity curve fits the observed one, and find the ratio of the computed amplitude of the light curve (ΔV_c) to the observed amplitude (ΔV_{obs}).
5. Repeat steps (2)-(4) for several q values.
6. If in step (1) the visible component was specified as the primary, specify it as the secondary (and *vice-versa*). Repeat steps (2)-(4) for several values of q.

The calculations in steps (3) and (4) are performed using the PHOEBE interface (Prša & Zwitter 2005) to the Wilson-Devinney code (Wilson & Devinney 1971).

In principle, using a relation between V, $B-V$ and stellar angular diameter θ (Kervella et al. 2004) would be more straightforward and simpler than calculating M^o_{bol} and T, and comparing M^o_{bol} to M^c_{bol} (note that T is needed for PHOEBE to derive M^c_{bol}). Based on such a relation, we could directly fit the "observed" radius of the visible component $R^o \equiv \theta D$ (where D is the distance to the cluster) to the calculated average radius of the Roche lobe. Unfortunately, fits of Kervella et al. (2004) proved to be unreliable when extrapolated to low metallicity and small θ. This is not surprising, as these authors explicitly warn about the nonlinearity of the relation involving V and $B-V$.

3.2. Discussion of errors

The values of our key input parameters, i.e. temperatures and bolometric luminosities, are not known accurately, and their errors are difficult to estimate without engaging in a lengthly (and likely ambiguous) discussion of involved factors. In order to verify how these uncertainties influence the output we varied T and M^o_{bol} by small amounts and observed the corresponding variations in m_1 and m_2. We found that decreasing T by 100 K causes the masses to grow by 7 − 10%, while an increase in M^o_{bol} by −0.1 mag makes them larger by 10 − 15%.

At a first glance, focusing on semi-detached systems seems too restrictive. To see it clearly, suppose that the visible component is entirely contained within its Roche lobe. Then in order to recover M^o_{bol} we would have to increase the orbital separation a. Since the period P is fixed, the masses would have to increase, too. To keep the observed velocity amplitude constant, the inclination i would have to decrease. For that reason, and also because the visible component would now be less deformed, ΔV_c would also decrease. This way the range of q for which the ratio $\Delta V_c/\Delta V_{obs} \approx 1$ could be extended onto fits which for semi-detached systems yield $\Delta V_c/\Delta V_{obs} > 1$. In principle, it is even possible that m_1 and m_2 derived for some mass ratio $q \neq q_b$ from detached fits could be smaller than $m^{sd}_1(q_b)$ and $m^{sd}_2(q_b)$. However, upon verifying this possibility we found that in most cases the detached fit results in either too low an amplitude for the light-curve or masses larger than those obtained for q_b, so that the extension of the q-range is marginal (if any). We conclude that the errors in the mass limits caused by neglecting detached configurations are smaller than those related to bolometric corrections or the color-temperature scale.

Another possible source of errors is the assumption that the whole light output of the system originates in the component responsible for the observed spectrum. The components of the only system in our sample in which two sets of velocities could be measured differ in brightness by $\Delta M \approx 1$ mag. Assuming that in the remaining systems $\Delta M = 2$ mag causes their brighter components to be dimmer by 0.16 mag. The corresponding de-

crease in masses, estimated from the general relation between mass and M^o_{bol} mentioned earlier, amounts to 15 – 20%.

3.3. Results

Quantitative results of the analysis are shown in Tables 3-13, and discussed in Sect. 3.3. The best fits are indicated with an asterisk in the last column of each table, and the corresponding computed light and velocity curves are displayed in Figs. 3, 4, 5 and 6, along with the observational data.

3.3.1. ω Centauri

V214. Assuming that the visible component is the secondary results in computed light-curve amplitudes consistently much too low. Assuming that it is the primary makes the difference between ΔV_{obs} and ΔV_c smaller, but still unacceptable.

In order to make ΔV_c larger, we are forced to look for solutions in which both components contribute to the observed ellipticity effect. Based on the simplest possible assumption that the system is in contact, we apply the following procedure: i) set q; ii) adjust a so that the combined M_{bol} of the system is 2.44 mag; iii) adjust i so that the computed velocity curve agrees with the observed one; iv) check if the computed light curve agrees with the observed one.

Table 3. Derived parameters for V214

q	a $[R_\odot]$	i [°]	m_1 $[M_\odot]$	m_2 $[M_\odot]$	$\Delta V_c/\Delta V_{obs}$
0.10	2.45	62	1.54	0.15	1.1
0.13	2.55	58	1.69	0.22	1.0*
0.15	2.60	47	1.76	0.26	0.6

The fits are shown in Table 3, and we conclude that the available data favor a system with a rather large mass ratio, which must have undergone significant mass transfer (and may still be transferring mass at a low rate). Obviously, the sum $m = m_1 + m_2$ should not exceed two turnoff masses of the youngest population of ω Cen, i.e. 1.84 $M_\odot$ (Norris 2004). Given the rather large errors in the mass estimates due to uncertainties in T and M^o_{bol}, one may accept that this requirement is fulfilled by at least the first two fits in Table 3.

V251. Like in the previous cases, assuming that the spectrum originates in the secondary we find that for all q values ΔV_c is much smaller than ΔV_{obs}. Assigning the spectrum to the primary leads to the results displayed in Table 4. As the total mass is markedly smaller than 1.84 $M_\odot$, we seem to have a system which not only underwent mass transfer, but also lost a significant amount of mass.

Table 4. Derived parameters for V251

q	a $[R_\odot]$	i [°]	m_1 $[M_\odot]$	m_2 $[M_\odot]$	$\Delta V_c/\Delta V_{obs}$
0.20	3.10	33	0.39	0.08	3.2
0.35	3.44	32	0.48	0.17	1.0*
0.50	3.67	22	0.52	0.26	0.65

V254. Assuming that the spectrum originates from the secondary leads once more to amplitude ratios $\Delta V_c/\Delta V_{obs}$ which for all mass ratios are much smaller than unity. Upon adopting that the source of the spectrum is the primary we get the results displayed in Table 5, which suggests that V254 is similar to V214.

Table 5. Derived parameters for V254

q	a $[R_\odot]$	i [°]	m_1 $[M_\odot]$	m_2 $[M_\odot]$	$\Delta V_c/\Delta V_{obs}$
0.2	2.77	72	1.61	0.32	1.7
0.3	2.98	43	1.84	0.55	1.0*
0.5	3.29	24	2.15	1.07	0.6

NV334. Because of the low brightness of the system (V = 18.83 mag) we were able to obtain only a very rough estimate of the velocity amplitude. We therefore modifed our analysis: we estimated the inclination based on the light curve, and compared the calculated velocity amplitude K_c to the observed one. Assuming that the spectrum originates in the secondary leads to K_c being much larger than K_{obs}, regardless of the value of q. The same analysis applied to the configuration with the primary generating the spectrum produces results shown in Table 6, which seem to indicate that NV334 is similar to V251. However, the similarity is superficial: the effective temperatures of the two systems differ by $\sim$ 4000 K, causing the cooler and dimmer NV334 to occupy an entirely different position in the color-magnitude diagram of ω Cen (see Fig. 1).

Table 6. Derived parameters for NV334

q	a $[R_\odot]$	i [°]	m_1 $[M_\odot]$	m_2 $[M_\odot]$	K_c/K_{obs}
0.1	1.22	76	0.33	0.03	0.4
0.3	1.45	65	0.47	0.14	1.2*
0.5	1.60	63	0.55	0.27	1.8

NV360. Our standard analysis fails for this system (iterations of the inclination i based on the velocity curve are either converging extremely slowly or entirely diverging), so that we again have to apply a modified version based on the light curve. As for the case of NV334, assuming that the spectrum originates in the secondary leads to K_c being much larger than K_{obs}, regardless of the value of q. Systems with the primary being responsible for the spectrum fare much better (see Table 7), and we conclude that NV360, unlike NV334, is truly similar to NV251.

Table 7. Derived parameters for NV360

q	a $[R_\odot]$	i [°]	m_1 $[M_\odot]$	m_2 $[M_\odot]$	K_c/K_{obs}
0.5	2.52	26	0.36	0.18	0.7
0.8	2.79	25	0.41	0.32	1.0*
0.9	2.86	25	0.42	0.37	1.1

NV400. When the secondary is assumed to generate the spectrum, the calculated light-curve amplitude is for all values of q

much higher than the observed one. Assuming that the spectrum originates in the primary we get the results displayed in Table 8. Apparently, NV400 is yet another system similar to V251.

Table 8. Derived parameters for NV400

q	a $[R_\odot]$	i [°]	m_1 $[M_\odot]$	m_2 $[M_\odot]$	$\Delta V_c/\Delta V_{obs}$
0.3	2.65	28	0.48	0.14	1.3
0.5	2.93	13	0.56	0.28	0.8*
0.8	3.24	9	0.63	0.50	0.2

V240. Assuming that the spectrum originates from the primary we obtain the results shown in Table 9: computed light-curve amplitudes are far too low (if the secondary were the source of the spectrum they would be even lower). Moreover, the total mass of the system is unacceptably high (as we argued in the case of V214, it should not exceed 1.84 $M_\odot$). In other words, the color and apparent magnitude of V240 are incompatible with its observed velocity amplitude, suggesting that this system does not belong to ω Cen. Another possibility is that the light of V240 is dominated by a tertiary component, and the recorded spectra are unrelated to the photometric binary.

Table 9. Derived parameters for V240

q	a $[R_\odot]$	i [°]	m_1 $[M_\odot]$	m_2 $[M_\odot]$	$\Delta V_c/\Delta V_{obs}$
0.07	2.83	16	2.59	0.18	0.1
0.1	2.96	11	2.88	0.29	0.05

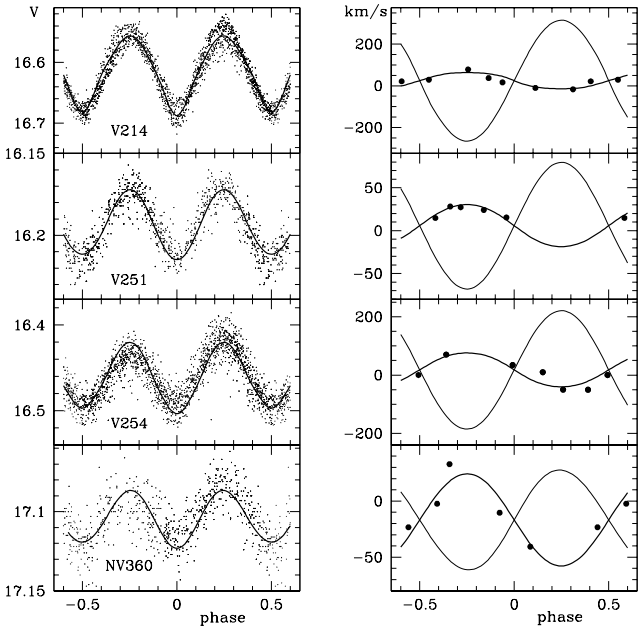

Fig. 3. Light and velocity curves of blue stragglers. Parameters of the plotted fits are given in Tables 3, 4, 5, and 7, in the rows indicated with an asterisk.

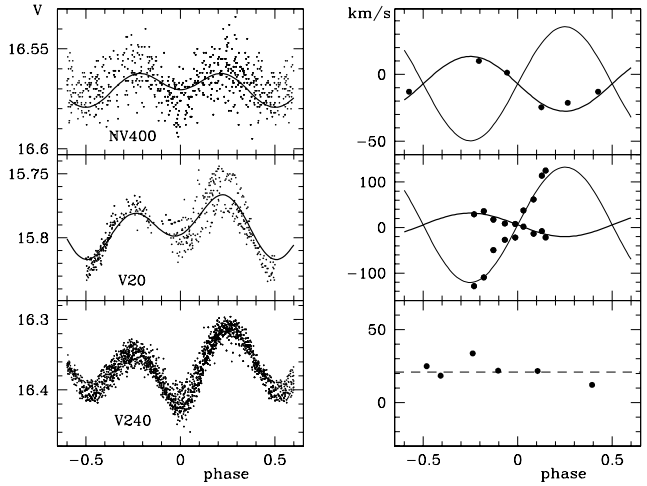

Fig. 4. Light and velocity curves of blue stragglers – continuation of Fig. 3. A single spot 2% hotter than the photosphere was placed on the primary of V20 in order to qualitatively account for the asymmetry of the light curve (just for illustrative purposes; it was not included while analyzing the data). Parameters of the fits for NV400 and V20 are given in Tables 8 and 11 in the rows indicated with an asterisk. No fit was possible for V240, because the velocity ampliutude turned out tobe smaller than the observational errors. The light curve, however, is coherent and remained stable between 1999 and 2003.

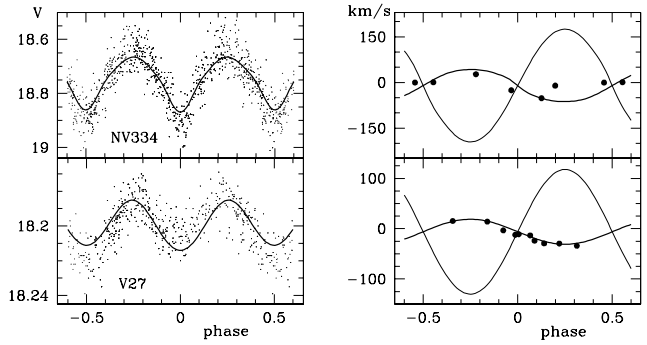

Fig. 5. Light and velocity curves of subdwarfs. Parameters of the plotted fits are given in Tables 6 and 12 in the rows indicated with an asterisk.

3.3.2. NGC 6397

V17. The visible component must be the secondary (an alternative assumption enforces inclinations at which, regardless of the value of q, the ratio $\Delta V_c/\Delta V_{obs}$ is much lower than unity). Our standard analysis produced the results shown in Table 10.

The fact that V17 is situated at the turnoff of the main sequence prompted us to consider an exceptional case of a detached binary with m_2 equal to the turnoff mass, which in NGC 6397 is close to 0.8 $M_\odot$ (Kaluzny et al. 2008). Keeping a conservative approach we set $m_2 = 0.75\ M_\odot$, and, as expected based on Table 10, we found that the amplitudes of all calculated light curves were too low. Our results indicate that the primary, although dimmer than the secondary, is rather massive, with a mass possibly exceeding 1 $M_\odot$.

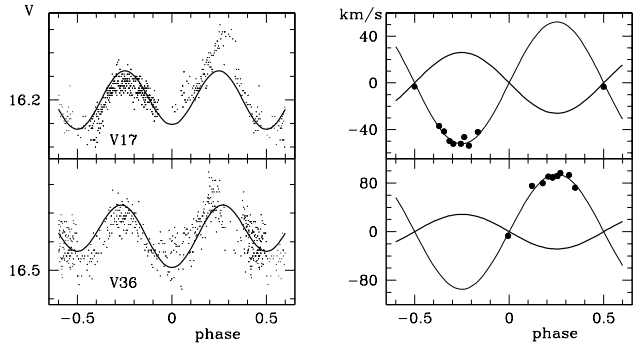

Fig. 6. Light and velocity curves of systems at the main sequence turnoff. Small ticks in light-curve plots are separated by 0.01 mag. Parameters of the plotted fits are given in Tables 10 and 13 in the rows indicated with an asterisk.

Table 10. Derived parameters for V17

q	a $[R_\odot]$	i [°]	m_1 $[M_\odot]$	m_2 $[M_\odot]$	$\Delta V_c/\Delta V_{obs}$
0.3	6.00	14	1.99	0.60	0.7
0.4	5.56	16	1.47	0.59	0.9
0.5	5.25	19	1.15	0.58	1.1*
0.6	5.02	21	0.95	0.57	1.5

V20. This is the only system in our sample for which it was possible to measure the velocities of both components. The measurements were performed using the TODCOR method developed by Zucker & Mazeh (1994), which also calculates the ratio of component fluxes $\alpha \equiv f_1/f_2$. Based on all available spectra of V20 (there were 9 of them), we obtained $\alpha = 2.47 \pm 0.02$ which, combined with $M^o_{bol} = 2.94$ mag, yields $M^o_{bol1} = 3.31$ mag and $M^o_{bol2} = 4.29$ mag.

Since the mass ratio is small ($q \approx 0.2$), the secondary must be rather oversized for its mass. We assume that it fills its Roche lobe, and we apply the following nonstandard procedure: i) set i; ii) iterate a and q to fit the velocity curves of both components); iii) adjust the size of the primary to get $M^c_{bol1} = 3.31$ mag; adjust the temperature of the secondary T_2 to get $M^c_{bol2} = 4.29$ mag (note that this is the minimum possible temperature). The best fit among those displayed in Table 11 indicates that V20 is another system similar to V251.

Table 11. Derived parameters for V20

i	a $[R_\odot]$	q [°]	m_1 $[M_\odot]$	m_2 $[M_\odot]$	$\Delta V_c/\Delta V_{obs}$
30	5.28	0.20	2.23	0.45	0.4
40	4.09	0.20	1.04	0.20	0.8
45	3.72	0.20	0.78	0.15	1.0*
50	3.43	0.20	0.61	0.12	1.2

V27. Upon applying the standard analysis we found that, regardless of whether the primary or the secondary produces the spectrum, for a given value of q either there is no inclination for which the calculated amplitude matches the observed one or the masses of both stars are unacceptably low ($m_1 \leq 0.05\,M_\odot$; $m_2 \leq 0.04\,M_\odot$). One can make them higher by assuming that the system is detached instead of semi-detached; however, in such a case it is impossible to find firm lower mass limits.

Table 12. Derived parameters for V27

q	a $[R_\odot]$	i [°]	m_1 $[M_\odot]$	m_2 $[M_\odot]$	T_2	$\Delta V_c/\Delta V_{obs}$
0.2	2.00	55	0.29	0.06	6500	1.0*
0.2	2.50	40	0.57	0.11	6000	0.9
0.2	3.00	33	0.98	0.20	6000	0.3
0.3	1.80	43	0.20	0.06	6000	0.9
0.3	2.00	36	0.27	0.08	6000	0.7
0.3	2.50	28	0.52	0.17	6000	0.2

To obtain a sample of detached solutions we modified our standard procedure in the following way: i) set q and a; ii) adjust i so that the calculated velocity curve agrees with the observed one; iii) adjust the size of the primary to get $M_{bol1} = 6.0$ mag; iv) adjust the size (and, if necessary, the temperature) of the secondary to get $M_{bol2} = 6.3$ mag (the latter two values are of course arbitrary, the only constraints being that the secondary is not much dimmer than the primary, and the combined bolometric magnitude of the system is 5.38 mag), v) check if the calculated light curve agrees with the observed one.

If one assumes that the spectrum is generated by the secondary, then the inclination consistent with the velocity curve is much too low to reproduce the light curve (except for systems with $q \gtrsim 0.75$, but in those cases the masses of the components are smaller than 0.05 $M_\odot$). The only reasonable solutions we were able to find for the detached configuration are based on the assumption that the primary generates the observed spectrum, while the secondary is mainly responsible for the observed ellipticity effect. The results shown in Table 12 seem to favor a configuration with small and rather discrepant masses.

V36. The visible component must be the secondary; the alternative assumption enforces inclinations such that the calculated amplitude of the light curve is much lower than the observed one for all values of q. However, assuming that the secondary fills its Roche lobe is untenable, as our standard analysis indicates that in such a case the calculated amplitudes of the light curve are too high. Thus, we are forced to adopt a detached configuration. Since V36 is located at the turnoff (only 0.3 mag below V17; see Fig. 2), we assume that $m_2 = 0.75\,M_\odot$ and apply the following four-step procedure: i) set q; ii) adjust a to get $m_2 = 0.75\,M_\odot$; iii) adjust i so that the calculated velocity curve agrees with the observed one; iv) adjust the size of the secondary to get $M_{bol2} = 3.65$ mag. The results shown in Table 13 indicate that V36 is similar to V17, with the primary's mass possibly even higher than 1.5 $M_\odot$.

Table 13. Derived parameters for V36

q	a $[R_\odot]$	i [°]	m_2 $[M_\odot]$	m_1 $[M_\odot]$	$\Delta V_c/\Delta V_{obs}$
0.2	7.40	20	0.75	3.77	0.9
0.3	6.62	24	0.75	2.49	1.0*
0.4	6.17	28	0.75	1.87	1.3
0.5	5.86	32	0.75	1.50	2.1

4. Discussion and conclusions

10 out of 11 objects in our sample exhibit radial-velocity variations indicating their binary nature (the only exception is V240 in ω Cen). In that sense, the sample was well chosen. Regarding the principal aim of the present survey we have been less successful - no clear-cut evidence for high-mass degenerate components was found. However, while 8 systems proved to be more or less ordinary binaries, the remainig two (V17 and V36 at the turnoff of NGC 6397) cearly deserve further scrutiny. First, they are the only systems in which the brighter component is the less massive secondary. Second, the masses of their dim primaries may be significantly larger than 1 $M_{\odot}$ (in V36, even larger than 2 $M_{\odot}$ if the secondary is indeed a turnoff-mass star). Third, they are weak X-ray sources. Based on Chandra observations, Bogdanov et al. (2010) classify them as active binaries (AB), i.e. systems composed of main-sequence or subgiant stars whose weak X-ray emission originates from magnetic activity. Our results rule out the possibility that they are composed of pristine stars which have not undergone any mass transfer episode, as in such a case the more massive component would also have to be the brighter one. This is not to say Bogdanov et al. (2010) are wrong: short-period degenerate binaries in quiescence may easily "masquerade" as AB systems, since they are most likely synchronized and their visible components spin fast enough for the stellar dynamo to be highly efficient.

According to the most optimistic interpretation of our results, V17 and V36 may contain a neutron star (the dim primary of V36 may even be a black hole). Such systems can indeed be expected, as population synthesis calculations indicate that the formation of a degenerate binary in which a neutron star or a black hole is accompanied by a main-sequence star or a subgiant is nothing unusual in globular clusters. Although the rate at which they form is not high ($<$ 2.5 systems/Gyr), they should be transient all the time, and therefore more likely seen as a qLMXBs rather than as bright LMXBs (Ivanova et al. 2008). Moreover, NGC 6397 belongs to core-collapse clusters for which the formation rates of Ivanova et al. (2008) are just lower limits. Another (admittedly, not too strong) support for the optimism comes from the detection of a possible qLMXB near the turnoff of M30 (Lugger et al. 2006). Main-sequence secondaries similar to those in V17 and V36 are also found in galactic X-ray binaries whose primary components are black hole candidates; e.g. V1033 Sco, GRS 1739–278 or V821 Ara (Ziolkowski, priv. comm).

The fact that all our blue stragglers except V240 are binary supports the currently leading hypothesis concerning the nature of these objects, namely that they result rather from an extensive mass exchange between the component stars than from stellar collisions (Knigge et al. 2009). In all cases the brighter component is the primary which according to the mass-transfer scenario must have acquired significant amounts of hydrogen-rich material from the envelope of the originally more massive secondary. In fact, our results seem to indicate that blue stragglers are Algol-like systems in which the original mass ratio has been reversed, causing the mass transfer to effectively stop. Our stragglers may be similar to the well-studied star V228 in 47 Tuc (Kaluzny et al. 2007), however we cannot exclude the possibility that in some of them the primary is already at the beginning of the subgiant branch and has become large enough to approach its Roche lobe.

V214 and V254 in ω Cen have primaries with masses likely exceeding 1 $M_{\odot}$ (maybe even 1.5 $M_{\odot}$), and their total masses approach 2 $M_{\odot}$. Systems that massive must have originated from binaries subject to conservative or nearly conservative mass transfer. They also have large amplitudes of light variations (0.12, mag and 0.10 mag, respectively), in our sample rivaled only by that of NV334 (~0.3 mag); however a significant contribution to this effect must originate from relatively large inclinations found for all three systems. The remaining blue stragglers are significantly less massive – their *total* masses are lower than 1 $M_{\odot}$. As far as we know, our results are the first to indicate such a broad (and possibly bimodal) mass distribution. If this effect is real, it probably reflects differences in the efficiency of mass transfer and/or mass loss. We note in passing that some mass may still be flowing between the components of V20, as this system exhibits an asymmetric and variable light curve, and is a weak X-ray source. Another possibility to account for the apparent large width of the mass distribution is related to the peculiarities of the chemical composition of ω Cen, in which strongly He-enriched subpopulations are suggested to exist, with Y reaching up to ~ 0.4 (e.g., Norris 2004; Piotto et al. 2005; but see also Catelan et al. 2010 for a recent review and some caveats).Our fits are based on the standard value $Y = 0.24$, and for a given $B - V$ color they can overestimate the temperature of enriched stars by up to a few hundred Kelvin (Dotter et al. 2008). If this is what happened, then our standard analysis caused the He-rich systems to artificially shrink both in size and mass. Such hypothesis would also explain why stragglers with signficantly different "apparent" masses are able to form a relatively tight group on the H-R diagram.

The subdwarfs NV334 and V27 are very similar to each other in that they have large mass ratios and low-mass primaries with practically the same effective temperatures. Our estimate of the primary's mass in NV334 is consistent with the canonical hot subdwarf mass of 0.47 $M_{\odot}$, while the estimated mass of the secondary falls near the peak of the mass distribution of the unseen companions to field hot subdwarf stars (Geier et al. 2009). On the other hand, and as pointed out by Moni Bidin et al. (2008), the close binary fraction among subdwarf stars appears to be much lower in GCs than in the field, which may point to different formation mechanisms for many of the GC subdwarfs. In V27 the estimated masses are significantly smaller (see Table 12); note however that they are also less reliable due to problems discussed in Section 3.3.2, and that the solution with $m_1 = 0.57\ M_{\odot}$ and $m_2 = 0.11\ M_{\odot}$ is also acceptable. Taken at face value, the starred parameters in Table 12 would indicate that V27 is very similar to HS 2231+2241, an HW Vir-type system with a companion at or below the very low mass limit for M-dwarfs. The $\sim 0.26\ M_{\odot}$ primary of HS 2231+2241 is a non-helium burning, post-RGB star (Østensen et al. 2008). Another example of such a type of star is the 0.24 $M_{\odot}$ component of HD 188112 (Heber et al. 2003). The primaries of NV334 and V27 are much cooler ($T \sim 7500$ K compared to $T = 28400$ K and $T = 20500$ K, respectively, for HS 2231+2241 and HD 188112), but this difference may result from their more advanced evolutionary stage.

Our sample is too small for a meaningful statistical analysis; nevertheless the above-discussed results indicate that further research on ellipsoidal binaries in globular clusters is a wortwhile task, and suggest its most promising direction: it seems that future sampling of the photometric variables should be biased towards objects located on or to the right of the main sequence, including those identified as weak X-ray sources. Obviously, for purely economical reasons (exposure times!) the targets sould not fall much below the turnoff point. Such an approach is tedious, but at the same time it is the only one on which a fair census of degenerate binaries in globular clusters can be based.

Acknowledgements. We are very grateful to Jay Anderson for providing HST proper-motion data for NGC 6397 and to Janusz Ziolkowski for a primer on black hole candidates in galastic X-ray binaries. Research of JK, PP and WP is supported by the grant MISTRZ from the Foundation for the Polish Science and by the grants N N203 379936 and N N203 301335 from the Polish Ministry of Science and Higher Education. Support for MC and CC is provided by MIDEPLAN's Programa Iniciativa Científica Milenio through grant P07-021-F, awarded to The Milky Way Millennium Nucleus; by Proyecto Basal PFB-06/2007; by FONDAP Centro de Astrofísica 15010003; and by Proyecto FONDECYT Regular #1071002. IBT acknowledges the support of NSF grant AST-0507325. We sincerely thank the anonymous referee whose remarks significantly improved the presentation.

References

Bellini, A., Piotto, G., Bedin, L. R. et al. 2009, A&A, 493, 959
Bogdanov, S., van den Berg, M., Heinke, C. O. et al. 2010, ApJ, 709, 241
Carretta, E., Bragaglia, A., Gratton, R. et al. 2009, A&A, 508, 695
Catelan, M., Valcarce, A. A. R. & Sweigart, A. V. 2010, in Star clusters: basic galactic building blocks, ed. R de Grijs & J. R. D. Lépine, IAU Symp. 266, 281
Clark, G. W. 1975, ApJ, 199, L143
Devecchi, B., Colpi, M., Mapelli, M. et al. 2007, MNRAS, 380, 691
Dotter, A., Chaboyer, B., Jevremović, D. et al. 2008, ApJS, 178, 89
Downing, J. M. B., Benacquista, M. J., Giersz, M., Spurzem, R. 2010, MNRAS, in press
Geier, S., Heber, U., Edelmann, H., et al. 2009, J.Phys.Conf.Ser., 172, 012008
Gendre, B., Barret, D., & Webb, N. A. 2003, A&A, 400, 521
Guillot, S., Rutledge, R. E., Bildsten, L. et al. 2009, MNRAS, 392, 665
Haggard, D., Cool, A. M., Anderson, J., et al. 2004, ApJ, 613, 512
Harris, W. E. 1996, AJ, 112, 1487
Heber, U., Edelmann, H., Lisker, T., & Napiwotzki, R. 2003, A&A, 411, L477
Ivanova, N., Heinke, C. O., Rasio, F. A. et al. 2008, MNRAS, 386, 553
Kaluzny, J., Olech, A., Thompson, I. B., et al. 2004, A&A, 424, 1101
Kaluzny, J., Thompson, I. B., Krzeminski, W., et al. 2006, MNRAS, 365, 548
Kaluzny, J., Thompson, I. B., Rucinski, S. M., et al. 2007, AJ, 134, 541
Kaluzny, J., Thompson, I. B., Rucinski, S. M., & Krzeminski, W. 2008, AJ136, 400
Katz, J. I. 1975, Nature, 253, 698
Kervella, P., Thévenin, F., Di Folco, E., & Ségransan, D. 2004, A&A, 426, 297
Knigge, C., Leigh, N., & Sills, A. 2009, Nature, 457, 288.
Lejeune, T., Cuisinier, F., & Buser, R. 1998, A&AS, 130, 65
Lugger, P. M., Cohn, H. N. Heinke, C. O. et al. 2006, ApJ 657, 286
Lynch, R., Ransom, S. M., Lorimer, D., & Boyles, J. 2010, BAAS, 42, 463
Maccarone, T. J., Servillat, M. 2008, MNRAS, 389, 379
Moni Bidin, C., Catelan, M., & Altmann, M. 2008, A&A, 480, L1
Munari, U., Sordo, R.m Castelli, F., & Zwitter, T. 2005, A&A, 442, 1127
Norris, J. E. 2004, ApJ, 12, L25
Østensen, R. H., Oreiro, R., Hu, H., et al. 2008, ASPC, 392, 221
Piotto, G., Villanova, S., Bedin, L. R., et al. 2005, ApJ, 621, 777
Pooley, D. 2010, PNAS, 107, 7164
Prša, A., & Zwitter, T. 2005, AJ, 628, 426
Remillard, R. A., & McClintock, J. E. 2006, ARA&A, 44, 49
Richer, H. B., Dotter, A., Hurley, J., et al. 2008, AJ, 135, 2141
Rucinski, S. M. 2002, AJ, 124, 1746
Sollima, A., Bellazzini, M., Smart, R. L., et al. 2009, MNRAS, 396, 2183
Stetson, P. B. 2000, PASP, 112, 925
Strickler, R. R., Cool, A. M., Anderson, J., et al. 2009, ApJ, 699, 40
Trager, S. C., King, I. R., & Djorgovski, S. 1995, AJ, 109, 218; erratum: 1995, AJ, 109, 1912
van der Marel, R. P. & Anderson, J. 2010, ApJ710, 1063
Verbunt, F., Pooley, D., & Bassa, C. 2008, IAU Symp., 246, 301
Villanova, S., Piotto, G., King, I. R., et al. 2007, ApJ, 663, 296
Weldrake, D. T. F., Sackett, P. D., & Bridges, T. J. 2007, AJ, 133, 1447
Wilson, R. E., Devinney, E. J. 1971, AJ, 166, 605
Zucker, S., & Mazeh, T. 1994, ApJ420, 806